Microscale Patches of Nonmotile Phytoplankton

Jorge Arrieta,[1,2] Ana Barreira,[2] and Idan Tuval[2]
[1]Área de Mecánica de Fluidos, Universidad Carlos III de Madrid, Madrid, Spain
[2]Instituto Mediterráneo de Estudios Avanzados, IMEDEA, UIB-CSIC, Esporles, Spain
(Received 4 December 2014; published 27 March 2015)

Phytoplankton cells have evolved sophisticated strategies for actively responding to environmental signals, most notably to mechanical stresses of hydrodynamic origin. A largely unanswered question, however, is the significance of these cellular responses for the largely heterogeneous spatial distribution of cells found in the oceans. Motivated by the physiological regulation of buoyancy prevalent in nonmotile phytoplankton species, we solve here a minimal model for "active" sinking that incorporates these cellular responses. Within this model, we show how buoyancy regulation leads to intense patchiness for nonmotile species as compared to passive tracers, resulting in important variations in settling speeds and, as a consequence, determining escape rates to the deep ocean.

DOI: 10.1103/PhysRevLett.114.128102 PACS numbers: 87.18.Hf, 47.63.-b, 92.20.Jt

Marine environments are dominated by scarce, patchy, and fast-fluctuating resource landscapes. This spatial heterogeneity plays an important role in ecosystem-level processes such as predator-prey interactions, ecosystem stability, and biological productivity [1]. For planktonic life forms, patchiness is a ubiquitous phenomenon for which oceanographic observations exist as early as the eighteenth century [2]. Physical and biological factors including growth and grazing together with large-scale oceanic turbulence contribute significantly to its formation [3–5]. However, there is still little consensus on its causes and consequences.

In recent years, significant effort has been devoted to understand the mechanisms underlying the formation of patches of marine phytoplankton [4], as these form the basis for the vast majority of aquatic food webs, are responsible for half of the world's oxygen production, and regulate essential biogeochemical cycles [6]. At the largest scales, phytoplankton cells behave as passive tracers advected by the oceanic flow, and patchiness mainly arises through the coupling of turbulence, population, and nutrients dynamics [5]. However, at smaller scales, when the velocities of the turbulent flow, according to the Kolmogorov energy cascade, become smaller the interplay between biological and physical factors becomes relevant, leading to the formation of unexpected macroscopic phenomena. These include the recently described generation of phytoplankton layers [7] or cell clustering [8,9] by gyrotaxis, an essential biophysical mechanism for swimming microorganisms. More generally, the hydrodynamics of motile microorganisms has been the subject of much recent theoretical [10,11] and experimental [12,13] work dealing with the intriguing properties of swimming at the lowest Reynolds numbers. On the contrary, our focus here is on nonmotile phytoplankton that comprise ecologically fundamental groups such as diatoms and cyanobacteria. Extensive work has already disproved the classical image of nonmotile phytoplankton as passive "wanderers" entrained by currents into a turbulent life. Indeed, nonmotile cells evolved sophisticated strategies for actively responding to environmental signals such as incident light, nutrient concentration, or mechanical stresses [14,15]. These cellular responses include changes in metabolic activity affecting cell buoyancy [16–21], variations of the cell cycle [22], triggering of cell-cell communication, and the initiation of cellular death [22–25].

First evidence that cellular activity produces changes in the density of phytoplankton cells was provided in Refs. [26,27], where it was shown that buoyancy was mainly controlled in diatoms by the replacement of heavy ions by light ions in the vacuole, whereas in cyanobacteria buoyancy is regulated by means of gas vesicles [28]. In either case, these physiological responses have a direct effect on the physical properties of the organism and, as such, they represent dynamical constraints that modify the interaction between the organism and its fluid environment in much the same way as motility does. However, the role of this relevant physiological response in the dynamics of phytoplankton sinking and its consequences for patchy distributions have been greatly overlooked. In this Letter, we build a minimal model for buoyancy control and show that changes in the density of the cell as a consequence of a physiological response to hydrodynamic stresses modify significantly the settling dynamics, leading to the appearance of intense patchiness for nonmotile species as compared to passive tracers, resulting in important variations in settling speeds and, as a consequence, determining escape rates to the deep ocean.

The problem of the motion of a sinking particle within a vortical flow is of great importance in diverse areas such as meteorology, manufacturing, energy production, or ecology. The seminal work of Stommel [29] dealt with the

sedimentation of noninertial particles within an array of vortices, showing that below a critical value of the still fluid particle sedimentation velocity, persistent suspension of heavy particles is possible. Above this critical value, the attraction regions (i.e., the so-called Stommel zones) disappear and all particles eventually settle. However, as was shown in Refs. [30,31], this trapping mechanism does not withstand inertial perturbations to the particles motion. Particle trapping is still possible in more complex turbulent-like scenarios due to the interplay between particle inertia and streamline curvature [32,33]. In this work, however, we stick to the simplest vortical case and highlight the effect of buoyancy control in the generation of stationary trapped solutions to the sinking dynamics.

We consider a well-known exact solution of the Navier-Stokes equations in the inertialess limit, the Taylor-Green vortex (TGV) flow [34,35], which consists of an array of counterrotating vortices with spacing L and a maximum vorticity ω_0 at their center. The doubly periodic velocity field is given by $\mathbf{u} = (\omega_0 L/4\pi)[-\cos(2\pi x/L)\sin(2\pi z/L), \sin(2\pi x/L)\cos(2\pi z/L)]$. For the low Reynolds number case considered here, $\mathrm{Re} = \omega_0 L a/(2\pi\nu) \ll 1$ with a the particle radius and ν the fluid kinematic viscosity, the dynamics of the inertial particles is determined by the Maxey-Riley equation [36]. For simplicity, we neglect the Basset history term and the Faxen corrections [37–39]. The nondimensional form of this equation is obtained by using the characteristic vortex length $L/(2\pi)$, time $1/\omega_0$, and velocity $\omega_0 L/(2\pi)$ scales and the maximum density of the particle ρ_0 to yield

$$(1-R/2)\rho_p \frac{d^2\mathbf{x}_p}{dt^2} = -[(1-R/2)\rho_p - R]\frac{v_s}{(1-3R/2)\mathrm{St}}\mathbf{k} + R\frac{D\mathbf{u}}{Dt} - \frac{1}{2}R\frac{d}{dt}(\mathbf{u}_p - \mathbf{u}) + \frac{1}{\mathrm{St}}(\mathbf{u} - \mathbf{u}_p), \quad (1)$$

where $\mathbf{x}_p$ represents the position of the particle, $\mathbf{u}_p$ its velocity, and $D\mathbf{u}/Dt$ the derivative along the path of a fluid element and $d\mathbf{u}/dt$ along the trajectory of the particle. Both derivatives are evaluated at the instantaneous position of the particle. Thus, motion of particles is controlled by three parameters: the particle Stokes number $\mathrm{St} = 2a^2\omega_0/(9\nu R)$ characterizing inertia, the material parameter R defined by the mass ratio $\rho_F/(\rho_0 + \rho_F/2)$, and the nondimensional still fluid sedimentation velocity of the particle $v_s = 2a^2 g(1-3R/2)/[9\nu R\omega_0 L/(2\pi)]$.

To model buoyancy changes upon mechanical stresses, we consider a linear dependence of the density of the particle with the local strain rate of the flow (which, for the TGV flow, is simply given by $\dot{\varepsilon} = 1/2\sin x \sin z$). This response is consistent with the nearly linear dependence shown in Ref. [14] for changes in the concentration of cytosolic calcium Ca^{2+} with applied strain rates in marine diatoms or the similarly linear physiological response with strain rate observed in bioluminescent dinoflagellates [40]. More generally, it can be considered as a first-order linearization of the cellular response to mechanical stimuli around ρ_0. As the detailed mechanism responsible for how intracellular responses translate into the regulation of buoyancy is still unclear and buoyancy changes were not directly characterized in those experiments, we will analyze two possible scenarios differing in the sign of the response: we refer to cells whose density decreases (increases) with applied stresses as *shear-thinning* (*shear-thickening*), respectively. Hence, density changes in the shear-thinning case reduce to $\rho_p = 1-2(1-\alpha)\beta|\dot{\varepsilon}|$, while $\rho_p = R/(1-R/2) + \beta[\alpha + 2(1-\alpha)|\dot{\varepsilon}|]$ for the shear-thickening case, with $\beta = (1-3R/2)/(1-R/2)]$ to allow for density changes in the observed range: from the maximum density of the cell to almost neutral buoyancy (i.e., a minimum sedimentation velocity set by the parameter α to αv_s) [6]. As we set the linearization by defining the density value at two different points (i.e., for the maximum $|\dot{\varepsilon}|$ and in the absence of mechanical stresses), the two cases are non-symmetric with respect to $|\dot{\varepsilon}|$. Although slightly more convoluted algebraically, this is an experimentally more accessible description. The limit $\alpha = 0$ corresponds to a particle that reaches neutral buoyancy, while $\beta = 0$ corresponds to passive particles with constant density, the sedimentation of which was amply considered in previous work [30,31]. Note that we assume an instantaneous response of the particle to changes in the strain rate, as the response time measured in Ref. [14] is on the order of $1-2$ s, while the time needed for sinking through the smallest vortex is on the order of minutes. A more complex response kinematics, including time-dependent buoyancy modulations and the resulting adaptive dynamics, will be the subject of future work.

We explore the effect of buoyancy control by integrating Eq. (1) for different values of the nondimensional parameters v_s, St, and R. Integration was carried out with a fourth-order Runge-Kutta scheme. Numerical results shown in Ref. [31] were used as a check for our numerical method. In particular, the mass-ratio parameter was fixed to $R = 0.4$ that corresponds to $\rho_0 = 2\rho_F$, which can be considered a good approximation of the maximum density of diatoms. We set $\mathrm{St} = 0.1$ and $\alpha = 0.1$. It should be noted that the Stokes number for a fixed value of the mass-ratio parameter depends on the size of the particle and the strength of the local flow, which eventually depends on the intensity of the vortical flow. The relative importance of the still fluid sedimentation velocity to the base flow is given by v_s. Thus, the most relevant phenomena arises when the sedimentation velocity of the particle is of the same order of the maximum velocity of the base flow (i.e., when $v_s \approx 0.5$). In Fig. 1 we compare the trajectories of passive, shear-thickening and shear-thinning particles for

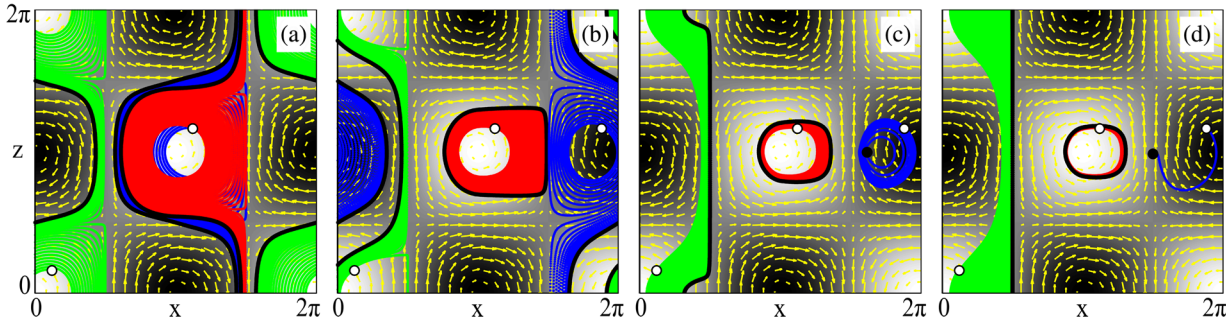

FIG. 1 (color online). Representative trajectories for $R = 0.4$, St $= 0.1$, $\alpha = 0.1$, and $v_s = 0.15$ (a), $v_s = 0.325$ (b), $v_s = 0.475$ (c), and $v_s = 0.525$ (d). In all panels and subsequent figures, the green lines (light grey) correspond to the passive case, the shear-thinning case is depicted in blue (dark grey), and the shear-thickening case is depicted in red (medium grey). All trajectories were initialized at the same (or equivalent in the doubly periodic domain) initial position (marked as a white circle) while the final steady state is marked in black. Background gray scale and arrows correspond respectively to the vorticity and velocity field of the Taylor-Green vortex flow.

different values of v_s around this value. All trajectories were initialized at the same (or equivalent in the doubly periodic domain) initial position (marked as a white circle in Fig. 1) and with the same initial velocity.

For small values of v_s the three trajectories are quite similar with particles reaching, after a transient time, a limit sinking trajectory, and no permanent suspension is possible [Fig. 1(a)]. As v_s increases, the effect of buoyancy control becomes more important: for $v_s = 0.475$ while all passive particles sink indefinitely, shear-thickening particles collapse into a limit cycle and shear-thinning particles converge to a stable fixed point along the $z = \pi$ line [Fig. 1(c)]. Both dynamical attractors are symmetric about the $x = \pi/2$ and $x = 3\pi/2$ lines. For $v_s > 0.5$, the dynamics of the passive and shear-thickening particles remains unaltered, while for the shear-thinning case the two symmetric fixed points along the $z = \pi$ line eventually collapse and a new pair emerges along the $x = \pi/2$ and $3\pi/2$ lines as shown in Fig. 1(d). Finally, for $v_s \gg 1$, all particles sink forever independently of their buoyancy control as long as we avoid the singular limit $\alpha = 0$. In this limit, the $z = \pi$ line degenerates, leading to nonphysical behavior with permanent suspension for arbitrarily large v_s.

To characterize the basin of attraction and, hence, the area of permanent suspension, we performed a parametric study of Eq. (1). Initial conditions were uniformly distributed within the domain $[0, 2\pi] \times [0, 2\pi]$, and integration was carried out for a sufficiently large integration time to safely discard slow transients. Figure 2(a) shows the area of attraction for different values of v_s for passive, shear-thinning, and shear-thickening particles. The vertical black dashed line marks the $v_s = 0.5$ condition. The results for passive inertial particles are consistent with previous work [30,31] and manifest the impossibility of permanent suspension under this simplified inertial scenario. In contrast, shear-thinning particles present a continuous transition to partial trapping with a maximum trapping area at $v_s = 0.5$, while shear-thickening particles show a discontinuous transition to global suspension at $v_s \approx 0.3$. The fundamental differences in potential trapping reported here for the first time highlight the relevance of buoyancy control for persistent suspension of nonmotile phytoplankton cells.

Moreover, and even when no permanent trapping is possible, buoyancy control has important consequences for the dynamics of sinking particles, substantially modifying sinking speeds and the duration of transients. To analyze the effect on sinking speeds, we calculate the mean asymptotic sedimentation speed for particles outside the basin of attraction as a function of v_s. Figure 2(b) shows the results for passive, shear-thinning, and shear-thickening particles. As was shown in Ref. [31], passive particles tend to display nonuniform spatial distributions under the combined effect of vortical advection, buoyancy, and inertia, preferentially converging to regions of low vorticity. This results, for low v_s, in an increase of the mean sinking speed $\langle v_z \rangle$ as compared to sinking in still fluid with particles exploring mainly the downwelling regions of the flow, but in a significant decrease in the mean sinking speed for $v_s \approx 0.5$ where sinking trajectories tend to the $x = \pi/2$ vertical line (as seen in Fig. 1). Buoyancy control

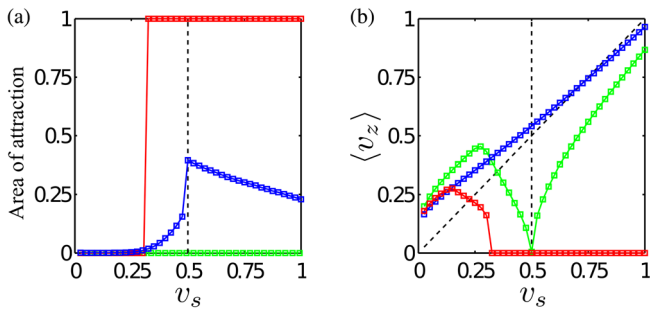

FIG. 2 (color online). The area of attraction (a) and the averaged sedimentation velocity of particles departing out of the area of attraction (b) for passive (light grey), shear-thinning (dark grey), and shear-thickening (intermediate grey) buoyancy control as function of the still fluid sedimentation velocity, v_s. The 45° dashed line in panel (b) is a visual guide for $\langle v_z \rangle = v_s$.

notably reduces sinking speeds for slowly sinking particles (i.e., $v_s \lesssim 0.3$) for both the shear-thinning and shear-thickening cases. For instance, passive particles sink twice as fast as shear-thickening particles for $v_s = 0.25$. On the contrary, mean sinking speed shows a marked decrease for passive compared to shear-thinning particles when $v_s \approx 0.5$ [see Fig. 2(b)]. These results emphasize that care should be taken when analyzing sinking speeds of nonpassive particles, as the interplay between advective contributions and physiological control translates into diverse forms.

We further explore the effect of buoyancy control on sedimenting particles by looking at the distribution of escape times to the deep ocean τ as a function of initial position $\mathbf{x}_p(t=0)$. We define operationally the escape time as the time needed for particles to cover a large vertical distance $z = 2\pi n$, with $n \gg 1$ to ensure we capture the asymptotic behavior. As shown in Fig. 3(b) for shear-thickening particles and v_s just below the discontinuous transition, the distribution is markedly bimodal with over an order of magnitude difference between the two distinct maxima. Hence, besides negligible particles trapping in this regime, the relative time spent by particles in suspension is highly heterogeneous when buoyancy control is included. On the contrary, the distribution of τ for passive particles is shown in Fig. 3(a) and presents a simple exponential decay for the same parameters used above. This dynamics can be better understood by observing the spatial distribution of escape times represented in Fig. 3(c). With over plotted black solid lines, we represent the trajectories of the attractive limit cycles that emerge above the transition. It is evident from this figure that particles departing within the area enclosed by the limit cycle take a significantly longer time to escape the initial periodic box, whereas particles with initial conditions outside of this area reach the attractive sinking trajectory more quickly.

The relevance of the described temporal heterogeneity for the emergence of spatially patchy distributions manifests in the accumulation index Ψ. Following the standard definition of patchiness used in spatial ecology [8,41], we partitioned the domain into N boxes and computed the normalized variance σ^2 over the mean μ of the box occupancy function to evaluate $\Psi = \mu + (\sigma^2/\mu) - 1$ for the stationary distribution. In Fig. 4(a) we highlight the linear covariation of St and v_s with a while keeping other physical parameters fixed. The effect of particle size on patchiness strongly depends on buoyancy control. While passive particles sink indefinitely and, hence, they do not contribute to the accumulation index of permanently suspended particles, the accumulation index for shear-thinning and shear-thickening cells is highly heterogeneous in parameter space. Ψ shows distinct maxima for cell sizes a in the range 10–100 μm, with the position of the maximum shifting towards lower radii as we consider smaller vortices. For turbulent oceanic flows and nonmotile species for which the described mechanism is prevalent, this would result in a cell size distribution within patches that depends on the intensity of turbulence as shown in Fig. 4(b): we expect small ($a \approx 10$ μm) nonmotile cells to dominate patchy distributions for typical turbulence conditions (where the size of dissipative vortices is given by a Kolmogorov scale $L_k \approx 10^{-3}$ m) while larger cells ($a \approx 100$ μm) will only display patchiness under more moderate turbulence (i.e., larger L_k). We are not aware of any field measurement to date either refuting or supporting this argument which, hence, remains as a testable prediction of our model.

In summary, we have presented the first study of the coupled dynamics of fluid advection and physiological buoyancy control in phytoplankton. Our results show that sinking dynamics in the ocean is qualitatively modified when active cellular processes are considered, with major consequences for the spatial distribution of cells, their sinking speeds, and their escape times to the deep ocean.

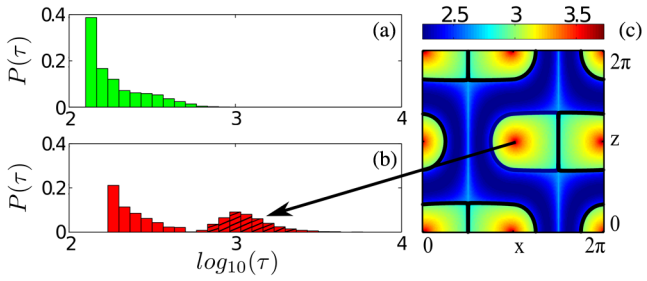

FIG. 3 (color online). The probability distribution of τ for (a) passive particles and (b) the shear-thickening case, with $v_s = 0.305$ and $n = 10$. (c) Contour plots of the spatial distribution of τ for the same parameter set. Trajectories plotted in black correspond with the four attractive limit cycles that emerge for $v_s \gtrsim 0.3$. Dashed (flat) filled bars in (b) correspond respectively to the distribution within (outside) the area enclosed by the black limit cycles shown in (c).

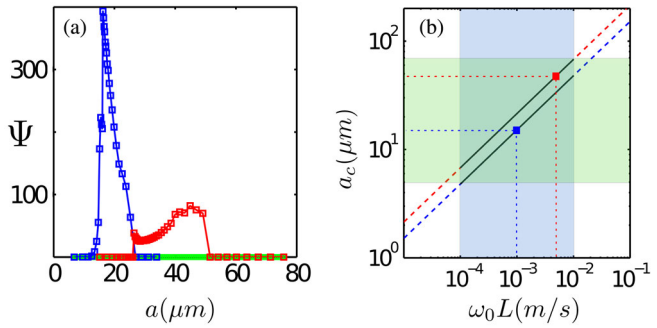

FIG. 4 (color online). (a) The accumulation index Ψ of permanently suspended particles as a function of particle radius a for passive (green line), shear-thinning (blue line), and shear-thickening (red line) buoyancy control. The different curves correspond to different scales within the Kolmogorov range as highlighted with squares in panel (b). The shaded area in (b) marks the typical range of values for the ocean.

This immediately suggests a number of specific experimental investigations. Chief among them is the detailed study of the cellular response function for representative phytoplankton species, using appropriately controlled mechanical stimuli coupled to tracking procedures to elucidate the sign, range, and time scales of natural responses. While simple vortical flows (such as the TGV flow used herein) provide fundamental insight of the most relevant physics, it is fundamental to assess the relevance of the proposed mechanism under more realistic spatially heterogeneous and time-dependent turbulent conditions either through direct numerical simulations of turbulent flows or by direct experimental visualization. Exploring these differences in future work may lead to important insights into the interplay of buoyancy control with dominant inertial processes that will help to clarify previous contradicting results on the fate of sinking particles [32,42,43]. Moreover, for certain microorganisms, the interplay between buoyancy regulation and motility, either in the form of stochastic or deterministic contributions, also requires further investigation. Additionally, the described dynamics is of interest for the burgeoning field of active matter where dense suspensions of motile cells are routinely used as a paradigmatic example, while active nonmotile cells have been hitherto ignored. Finally, our results suggest the possibility of engineering solutions for the permanent suspension of heavy particles in turbulent flows based on active buoyancy control, with a wealth of applications in the microfabrication industry.

We acknowledge the financial support of the European Union Seventh Framework Programme (FP7/2007-2013) under Grant No. FP7-PEOPLE-2011-CIG No. 293638, the Spanish Ministry of Economy and Competitiveness Grant No. FIS2013-48444-C2-1-P and from the subprogram Ramón y Cajal (IT).

[1] P. Legendre and M.-J. Fortée, Vegetatio **80**, 107 (1989).
[2] R. Bainbridge, Biol. Rev. Camb. Philos. Soc. **32**, 91 (1957).
[3] D. H. Turpin and P. J. Harrison, J. Exp. Mar. Biol. Ecol. **39**, 151 (1979).
[4] A. P. Martin, Progr. Oceanogr. **57**, 125 (2003).
[5] Z. Neufeld and E. Hernandez-Garcia, *Chemical and biological processes in fluid flows. A dynamical systems approach* (Imperial College Press, London, 2009).
[6] C. S. Reynolds, *The ecology of phytoplankton* (Cambridge University Press, Cambridge, England, 2006).
[7] W. M. Durham, J. O. Kessler, and R. Stocker, Science **323**, 1067 (2009).
[8] W. M. Durham, E. Climent, and R. Stocker, Phys. Rev. Lett. **106**, 238102 (2011).
[9] W. M. Durham, E. Climent, M. Barry, F. De Lillo, G. Boffetta, M. Cencini, and R. Stocker, Nat. Commun. **4**, 2148 (2013).
[10] E. Lauga and T. R. Powers, Rep. Prog. Phys. **72**, 096601 (2009).
[11] J. S. Guasto, R. Rusconi, and R. Stocker, Annu. Rev. Fluid Mech. **44**, 373 (2012).
[12] K. Drescher, R. E. Goldstein, N. Michel, M. Polin, and I. Tuval, Phys. Rev. Lett. **105**, 168101 (2010).
[13] J. S. Guasto, K. A. Johnson, and J. P. Gollub, Phys. Rev. Lett. **105**, 168102 (2010).
[14] A. Falciatore, M. R. d'Alcalà, P. Croot, and C. Bowler, Science **288**, 2363 (2000).
[15] A. Falciatore and C. Bowler, Annu. Rev. Plant Biol. **53**, 109 (2002).
[16] T. J. Smayda and B. J. Boleyn, Limnol. Oceangr. **10**, 499 (1965).
[17] T. J. Smayda, Limnol. Oceangr. **19**, 628 (1974).
[18] V.S Smetacek, Marine biology **84**, 239 (1985).
[19] A. M. Waite, Ph.D. Thesis, The University of British Columbia, 1992.
[20] T. A. Villareal, J. Plankton Res. **14**, 459 (1992).
[21] T. L. Richardson and J. J. Cullen, Mar. Ecol. Prog. Ser. **128**, 77 (1995).
[22] R. Casotti, S. Mazza, C. Brunet, V. Vantrepotte, A. Ianora, and A. Miralto, J. Phycol. **41**, 7 (2005).
[23] A. Vardi, F. Formiggini, R. Casotti, A. De Martino, F. Ribalet, A. Miralto, and C. Bowler, PLoS Biol. **4**, e60 (2006).
[24] D. L. Kirchman, Nature (London) **398**, 293 (1999).
[25] K. D. Bidle and P. G. Falkowski, Nat. Microbiol. Rev. **2**, 643 (2004).
[26] F. Gross and E. Zheuten, Proc. R. Soc. B **135**, 382 (1948).
[27] L. W. J. Anderson and B. M. Sweeney, J. Phycol. **14**, 204 (1978).
[28] A. E. Walsby, Microbiol. Rev. **58**, 94 (1994).
[29] H. Stommel, J. Mar. Res. **8**, 24 (1949).
[30] M. R. Maxey and S. Corrsin, J. Atmos. Sci. **43**, 1112 (1986).
[31] M. R. Maxey, Phys. Fluids **30**, 1915 (1987).
[32] C. Pasquero, A. Provenzale, and E. A. Spiegel, Phys. Rev. Lett. **91**, 054502 (2003).
[33] R. Sciascia, S. De Monte, and A. Provenzale, Phys. Lett. A **377**, 467 (2013).
[34] G. I. Taylor, Philos. Mag. Ser. 5 **46**, 671 (1923).
[35] P. Drazin and N. Riley, *The Navier-Stokes equations. A classification of flows and exact solutions* (Cambridge University Press, Cambridge, England, 2006).
[36] M. R. Maxey and J. J. Riley, Phys. Fluids **26**, 883 (1983).
[37] A. Provenzale, Annu. Rev. Fluid Mech. **31**, 55 (1999).
[38] A. Babiano, J. H. E. Cartwright, O. Piro, and A. Provenzale, Phys. Rev. Lett. **84**, 5764 (2000).
[39] A. Daitche and T. Tél, New J. Phys. **16**, 073008 (2014).
[40] P. von Dassow and M. I. Latz, J. Exp. Biol. **205**, 2971 (2002).
[41] M. Lloyd, J. Anim. Ecol. **36**, 1 (1967).
[42] J. Davila and J. C. R. Hunt, J. Fluid Mech. **440**, 117 (2001).
[43] J. Ruiz, D. Macías, and F. Peters, Proc. Natl. Acad. Sci. U.S.A. **101**, 17720 (2004).